https://doi.org/10.2352/ISSN.2470-1173.2019.11.IPAS-255

Gradient Management and Algebraic Reconstruction for Single Image Super Resolution

Leandro Morera Delfin, email:lmorera@cenidet.edu.mx, Center of Investigation and Technological development CENIDET, Morelos, Mx Raul Pinto Elias, email: rpinto@cenidet.edu.mx, Center of Investigation and Technological development CENIDET, Morelos, Mx Humberto de Jesús Ochoa Domínguez, email: hochoa@uacj.mx, Universidad Autónoma de Ciudad Juárez, UACJ, Chihuahua, Mx

Abstract

In this paper, a single image multi-scale super-resolution technique is proposed. The concept under study is the learning procedure between steps of amplification in order to predict the next high scale of resolution. The method integrates two different approaches for the prediction of a high resolution multi-scale scheme, a pure interpolation and a gradient regularization. In the first step a pure interpolation is carried out. It is used a prediction scheme with algebraic reconstruction through different scales to produce the high resolution output. In the last step, the residual blur is reduced by a gradient auto-regularization method. The gradients are adapted by using a weight in a neighbour. Precision of method can be controlled by the parameters of an algebraic reconstruction technique (ART). The proposed model avoids the fast decrease of the output resolution as the amplification factor increases. The proposed system was tested with a dictionary. Results show that the output image quality is improved despite of the increment of the scale factor.

Introduction

The procedures for single image's super resolution (SR) can be divided into: pure interpolation, employ of dictionaries and reconstruction methods. The common goal of these techniques is to yield an image as if it had been acquired with a high resolution physical device. The interpolation for amplification purposes is based on physical principles, for example, optical models can be modeled with amplification kernels, given by the Fourier transform of a truncated sampling array [1]. Some methods of pure interpolation, like the curvature interpolation method (CIM), studies the edge composition of the low resolution image to interpolate the curvature to a high-resolution (H_r) domain. The CIM constructs the high-resolution image by solving a linearized curvature equation, incorporating the interpolated curvature as an explicit driving force [2]. Other regression-based image interpolation algorithms, use an objective function optimized by ordinary least squares (OLS). However, it has been shown that interpolation with OLS may have some undesirable properties from a robustness point of view, for example, even small amounts of atypical values can dramatically affect the estimates results [3–6].

Interpolation-based methods [7–11] yield zoomed-in images with visual artifacts such as ringing, aliasing, blocking and blurring. The Fourier transform of the truncated sampling array is an interpolation kernel and can be a filter with maximum response of amplitude at high spatial frequencies. An optimal amplification kernel can be reached by using the high frequency content at high-resolution image domain as an explicit driving force for the variation of the amplification kernel parameters.

In the learning-based SR methods [12,13,16] the correspondences between low resolution L_r and high resolution H_r image patches are first learned from a database. The the system is applied to a new L_r image to recover its H_r version. With these methods, improved performances have been reported compared to traditional SR methods [17,18]. However, these methods rely largely on the quality of the prior images, that is, in the similarity between the training set and the test set. The dictionary methods are expensive in terms of number of operations due to the large training set used [19,20]. Recently, residual learning techniques exhibit improved performance, in [14] the performance is further improved by expanding the model size while the training procedure is stabilized, the authors can reconstruct high-resolution images of different up-scaling factors in a single model [15].

The reconstruction-based methods need a constraint [21,22], which requires that the downscaled version of the target H_r image be close to the L_r image. However, these methods yield reconstructed edges that can be too sharp and look unnatural. The edge-directed SR models [23–28] estimate the H_r image by enforcing some edge knowledge, such as the smooth edge [24,25,27] or the gradient profile prior (GPP) [23,28]. The enforced edge knowledge have some difficulties. The smooth edges for small scales could not be recovered in H_r and the GPP is learned from an image data set, therefore the similarity dependence is present.

In natural images, the local patterns repeat within and across the scales [29]. The multi-scale self-similarities, sparse representation and structural distribution have been exploited [30,31]. For example, in the work proposed by Buckstein et al. [30], the gradients of the image are not regularized and some restriction can be required to increase the quality of the H_r image. Dong et al [31], proposed a rigid regression technique, forcing a solution over groups of similar patches exploiting the redundancies of the image and introducing tree elements in the procedure. The first element is the gradient of the H_r image, conserved by adapting the gradient histogram of the image. The remaining elements are the energy norm and coefficient similarity decomposition.

In this work, a SR method that learns the next scale of amplification by preserving the relative position of the super imposed patches in previous scales is proposed. The procedure uses a convergent algebraic reconstruction technique (ART) in a cross inter-scale representation. Also, the multi-scale similarity redundancy is exploited in the image's gradient auto-regularized domain. The main contributions of our SR method are summarized next:

- A decreasing of the blur at the output step of a multi-scale magnification using auto-regularized gradient domain.
- Adaptive convergence to the high resolution with ART in a

transverse plane of the multi-scale magnification scheme.
- Detection of the gradients with maximal step ascend-descend algorithm around the inflection points in all directions for the auto-regularized gradient procedure.

The remainder of this paper is organized as follows. Related work are reviewed. The proposed auto-regularization procedure is explained and the multi-scale scheme of interpolation explained, detailed description of the proposed SR algorithm with ART convergence in a multi-scale scheme is provided and finally the results are analyzed.

Related work

The classical model for the simulation of a degraded image uses a degradation matrix H and additive noise v over a H_r image x:

$$y = H \cdot x + v \tag{1}$$

In SR via dictionaries, overlapped patches of size mxm are extracted by using an extraction matrix R of dimension mxM. The amount of pathes in an image of size MxM is equal to $(M-m/2+1)*(M-m/2+1)$. When a dictionary ϕ is employed and a transference function α^y is found by some procedure like $K-SVD$ [32], the estimated image can be reconstructed as:

$$\hat{x} = \phi \cdot \alpha^y = \left(\sum_{i=1}^{l} R_i^T \cdot R_i \right)^{-1} \sum_{i=1}^{l} \left(R_i^T \cdot \phi \alpha_i^y \right) \tag{2}$$

Equation (2) pretends to learn an universal over-complete dictionary to represent image structures [33]. However, sparse decomposition over a highly redundant dictionary is potentially unstable, and is scale dependent. Also, the redundancy of the patches is a probabilistic term that cannot be ignored. The redundancy and probabilities of occurrence of similar patches are other negative aspects in relation to deterministic procedures. The question is how to contribute from two points of view: dictionary learning and the optical principles of the amplification of the image. A H_r image can be expressed by sub-scales using some transfer function. This function needs to be found between patches of different scales where a light beam is only in a pixel position. The patch at position i, j belongs only to an image X_s at the scale n.

Proposed Model

For a L_r image an inter-scale lineal system is constructed, since there are patches of the image where a light beam is passing at different distances or scales. The input L_r image and its degraded versions can be used to construct the L_r to H_r multi-scale scheme. Considering different sizes of the L_r and H_r images, the L_r input y is enlarged to the same size of the H_r image x using bicubic interpolation, it is also a blurred and downscaled version of the H_r image x. Therefore,the correspondence between the L_r and H_r images at the same scale is established as follows:

$$z = (y) \uparrow s = ((x \star G) \downarrow s) \uparrow s = E_s x \tag{3}$$

Where $\star$ is the convolution operator, $\uparrow s$ is the upsampling operator with the scaling factor s, $\downarrow s$ is the downsampling operator with the scaling factor s, G is a blurring kernel (*e.g.*, an isotropic Gaussian kernel with the standard deviation σ), E_s is an operator composed of blurring, downsampling and upsampling with scaling factor s; y is the L_r image, x is the H_r image, and z is the L_r image at the same size of x. Note that the L_r image is more similar to its H_r image version when the scaling factor is small, whereas the high-frequency details tend vanish when the scaling factor is large. In our system, we adopt the multi-step magnification scheme with ART for the estimation of the target H_r image. For a L_r input image y with a total scaling factor d, the number of magnification steps is determined as $M = \log(d)/\log(s)$. Specifically, the relationship between the H_r image (x_{sm} at the m-th scale) and the H_r image ($x_{s,m+1}$ at the $(m+1)^{th}$ scale) can be expressed as follows:

$$x_{s,m} = \left(x_{s,m+1} \star G \right) \downarrow s \tag{4}$$

Equation (4) in the multi-scale case can be written in the form:

$$z_{s,m} = ((x_{s,m} \star G) \downarrow s) \uparrow s = E_s x_{s,m}. \tag{5}$$

Where L_r, the input image (y), is regarded as the H_r image x_{s_0} at the scale $m = 0$. Specifically, the H_r image x_{s_0}, from the interpolation process, is blurred and down-sampled to generate the images x_{s_m} at the scales m = 1,...,N. The L_r image z_{s_0} is produced by blurring and down-sampling the H_r image x_{s_0} and then upsampled the down-sampled result by bicubic interpolation. The procedure is shown in Figure 1.

Algebraic Reconstruction Technique

A multi-scale model as [37] uses the similarity of patches [36] in previous scales of the image to estimate an amplified image using a rigid regression. The transfer function found is passed to the input image together with its previous scales. The use of similarities incorporates a probability factor [36]. The proposed method maintains the localization by which the light beam were passing in the acquisition process and the ART minimization technique is used as a solution. For that, the image is crossed between scales and only the pixel values in the same position and at different scales are used to estimate the coefficient of lineal dependency for the reconstruction of the H_r image. A direct transition to a high scale can yield inaccurate results due the large transition in the gradients for very high scales of amplification. The pure interpolation (PI) process yields different dimensions at which the variations of the image are maximized. We call these scales the intermediate scales and consider this procedure are a step in a multi-scale prediction system. The goal is to incorporate a convergence method learning inter scales. Figure 2 shows the process by which a bi-cubic interpolation is used from the scales 1....n to obtain the scale $n+1$. The system is built in a patch by patch mode and solved by the ART model as the 2 shows . In our case, M rays pass through the correspondent patches p of dimensions $m \times m$ at location (i, j). The rays are perpendicular to the sequence of images in an incremental order of resolution. The interjection of the ray $M(m1, m2)$ with each correspondent pixel $(m1, m2)$ of

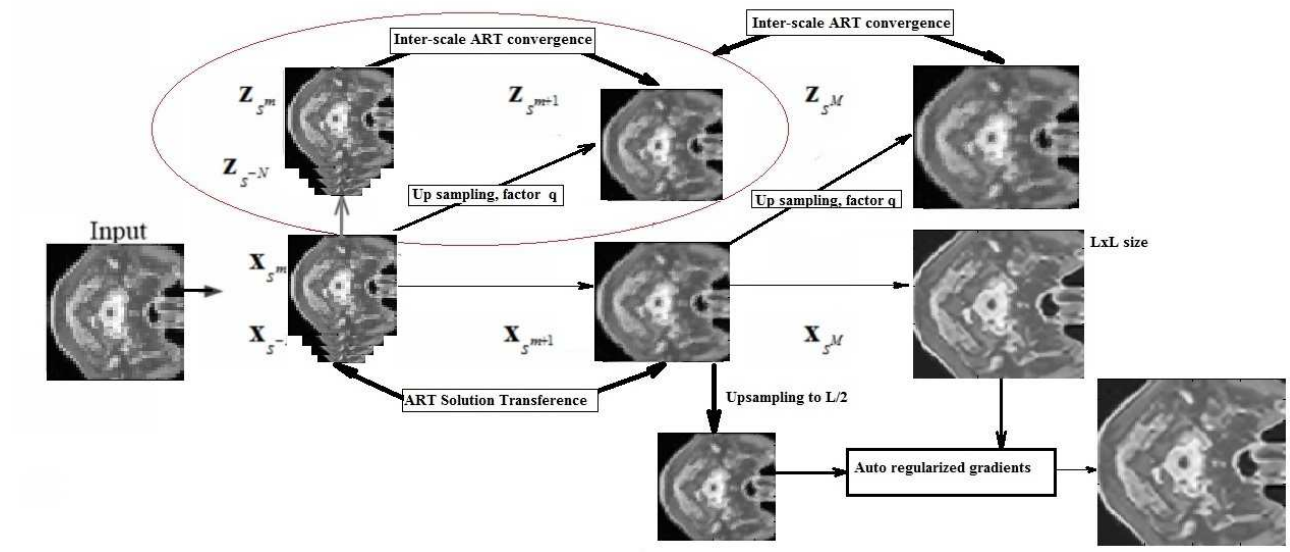

Figure 1. *Proposed SR model*

the patch i, j at scale n are integrated and a solution for a lineal dependence is found at the next scale using the *ART* model. In this paper, each scale of the image is considered as a dimension in the space and a number M of light beam are passing through the images at different scales. The relationship between the scale functions f defined by the values of the image at the scale j, the values of the pixel of the patches at different scales and the high resolution image is of the form.

$$\sum_{j=1}^{N} w_{i,j} f_j = p_i \tag{6}$$

The weight factor $w_{i,j}$ is equal to the fractional area of a pixel at the j^{th} scale of the image intercepted by the i^{th} ray as shown for one of the patches in the figure 2. Then the p_i term is the desired pixel value at the H_r image. A grid representation with a number of N cells gives an N degrees of freedom in an image. Therefore, a patch of the images Z_s of the Figure 1, represented by lineal combination of the previous scales (f_1, f_2,....., f_N), may be considered a single point in an N scale. Selecting super imposed patches of four pixels in the image, $M = N = 4$, and the system can be spanned as:

$$\begin{bmatrix} w'_{1,1}f_1 & w'_{1,2}f_2 & w'_{1,3}f_3 & w'_{1,4}f_4 \\ w'_{2,1}f_1 & w'_{2,2}f_2 & w'_{2,3}f_3 & w'_{2,4}f_4 \\ w'_{3,1}f_1 & w'_{3,2}f_2 & w'_{3,3}f_3 & w'_{3,4}f_4 \\ w'_{4,1}f_1 & w'_{4,2}f_2 & w'_{4,3}f_3 & w'_{4,4}f_4 \end{bmatrix} \cdot \begin{bmatrix} c_1 \\ c_2 \\ c_3 \\ c_4 \end{bmatrix} = \begin{bmatrix} p_1 \\ p_2 \\ p_3 \\ p_4 \end{bmatrix} \tag{7}$$

$$w_{i,j} = w'_{i,j} \cdot c_j \tag{8}$$

The solution is carried out by the method of projections shown in Figure 2. When a solution is attained, the transfer function is used to solve a lineal system using the input image patches extracted from the images X_s of the figure1, the lineal combination of the sub-scales using Equation 6 and the coefficients c_j produce the H_r patches of the output image.

The model of ART uses the following equations in a cross-scale model.

$$\overrightarrow{f}_i = \overrightarrow{f}_{i-1} - \frac{f_{i-1} * w_i - p_i}{\overrightarrow{w}_i * \overrightarrow{w}_i} * \overrightarrow{w}_i \tag{9}$$

$$\varepsilon \leq | \overrightarrow{f}_i - \overrightarrow{f}_{i-1} | \tag{10}$$

Where p_i is the desired intensity of the image in the higher scale of the up sampled band and f_{i-1} the previous image obtained in the iterative process, w_i are the pixels areas by where the light beam is passing as showed in figure 2 into a patch of *mxm* at the scale i.

Auto-Regularized Gradients

For large scales of amplification the blur effects of PI are more evident. In our work an auto-regularization gradient (ARG) method is used to improve the edges of the H_r output image after the inter-scale ART reconstruction. The edges of the H_r image are found by using the first derivative in the x and y directions. Afterwards, the second derivative is calculated and the inflection points around the edges are found. The amount of pixels between the inflection points is considered as the width of the edge. The edges are then interpolated using the magnitude of the second derivative and an average of the curves width in a neighbourhood [35]. Figure 3 shows how the edge is restored by sharpening it. A displacement (green arrows) in the position of the values of the first derivative is guided by zero-crossing of the second derivative. For the width of the edge the maximal ascent or descent gradient direction is found from the zero crossing to the first local maximum and the first local minimum of the second derivative with those data a curve factor (k) is calculated. The curve scale factor is adaptive and depends on the average of the curve width around an

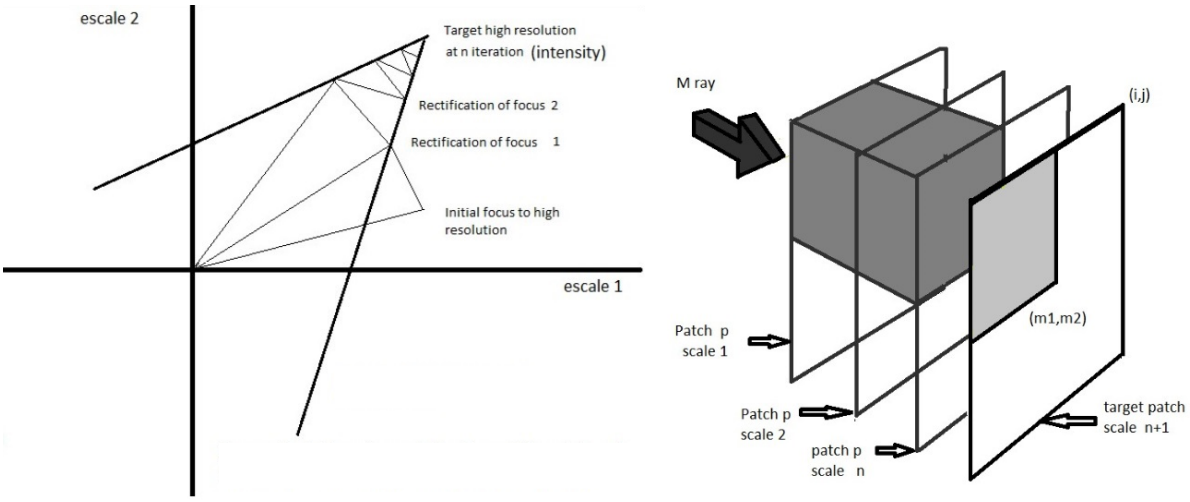

Figure 2. *Geometric interpretation of the ART procedure for convergence to the next H_r image and example of patches at different scales that converge to a H_r image, the black arrow represents the transverse light beam .*

edge. The inflection points and the mean width of the edge are used to calculate k to relate the gradient of the contour and the displacement.

The super-resolved image is obtained by minimizing a multivariate restricted function in the negative gradient direction [35, 36]. Two restrictions are considered [35], the differential of the gradient and the difference of the image with the previous scale. The scale factor of the curve k and the iteration in equation (11) are selected by closing the distance between gradients of the H_r output image of the multi-scale SR system and the previous scale $X_{s_{m-1}}$ in the proposed model of the Figure 1.

$$I_{h,k}^{t+n\tau} = I_{h,k}^{t+(n-1)\tau} - \tau \cdot \begin{pmatrix} \left(\left[\left[I_{h,k} \otimes g \right]_{\downarrow} (\beta) - I_l \right]_{\uparrow} (\beta) \right) \otimes g \\ -\alpha(div(\nabla I_h) - div(\nabla \hat{I}_{h,k})) \end{pmatrix} \tag{11}$$

$$\varepsilon \leq || \, I_{h,k}^{t+n\tau} - I_{h,k}^{t+(n-1)\tau} \, ||_2 \, . \tag{12}$$

Where n is the iteration number and $\otimes$ the convolution operator. $\hat{I}_{h,k}$ is the result of the interpolation method, I_l is the low resolution image, g is a low pass filter before decimation factor β. After exhaustive tests α and τ are selected to be 0.129.

Results

The following experiments were carried out with the proposed system. First, a longitudinal study of the brain with magnetic resonance imaging (MRI) at the acquisition time T_2 was used. The volume size was $180 \times 217 \times 180$ voxels. The slices were filtered using a Butterworth filter with a cutoff frequency of π/q and were sampled down by a factor of q to obtain a slice size of 90×109, then, this low resolution image was amplified. In another case, the BSDS500 database was used for comparison purposes and a dictionary technique [34] to improve the final results. In addition, the BSD100 database also was used for comparative purposes. The results of the multiscale ART scheme plus self-regulated gradients are compared with some pure interpolation methods. The ART-AG model provides a good response for high amplification scales and improves the results of the dictionary-based SR method.

Multiscale Scheme with Auto-Regularized Gradients

The ARG method is applied to the output of the ART multiscale scheme. In parameters selection k is adapted to the amplification scale as in [35]. The blue curve of the figure 3, is the gradient of high resolution. A sharper and amplified slice is obtained with the curve factor k and n iteration, it is shown in the right side of the figure 3 with a k swept from 1.7 to 2.3 with increments of 0.1 and reconstruction iterations from 1 to 5. The increment of SSIM respect to an original H_r image is important for MRI studies because the resolution is highly dependent of the magnetic field applied.

Algorithm

- Design the ART model with the necessary sub-scales and determine the transfer function of the system in the up sampling stair. Use the equation 3.
- Select the patches for ART processing from the image of major scale using the equation 2
- Select the number of iteration of the process for the ART precision shown in the equation 10.
- Solve the ART model and apply the solution of the system for a lineal dependence of the input image and the down sampled versions. Use the equations 9 and 10.
- Make an up sampled version of the input image of the middle off the output dimensions of the ART transfer system using the equation 6.
- Optimize the ARG model using the parameters: iteration, zero crossing, neighbourhood and curve factor. Use the equations 11 and 12.

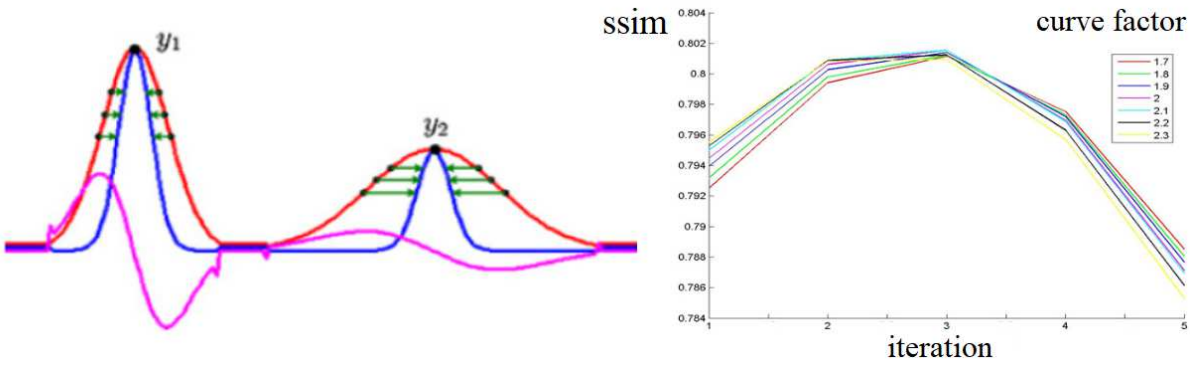

Figure 3. *Example of edge sharpening with auto regularized gradient. The red curve is the original gradient magnitude (first derivative), the pink curve is the second derivative and the blue curve is the resulting sharpened edge. Right side, graphic of iteration of reconstruction vs SSIM.*

SSIM results for different iterations (it) and k parameter

			k				
It	1.7	1.8	1.9	2	2.1	2.2	2.3
1	0.7928	0.7998	**0.8016**	0.7979	0.7888	0.7748	0.7564
2	0.7935	0.8002	**0.8016**	0.7977	0.7883	0.7741	0.7555
3	0.7943	0.8007	**0.8018**	0.7976	0.7880	0.7735	0.7547
4	0.7947	0.8008	**0.8018**	0.7973	0.7875	0.7728	0.7539
5	0.7953	0.8011	**0.8017**	0.7969	0.7869	0.7720	0.7529

Note: Bold values indicate the best result

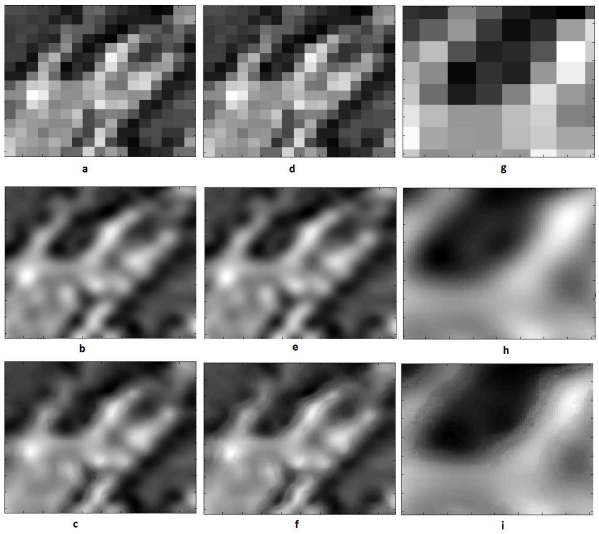

Figure 4. *Details of the slice four, (a) and (d) low resolution slice. (b) and (e) Proposed ART multiscale scheme, (c);ART+ARG with k = 1.2 and (f) ART+ARG with k = 3, it =5.*

ART convergence results

The multiescale model is build by using down sampled scales and one up sampled scale. The up sampled process is made using bicubic interpolation. Figure 5 shows the sub-scales and up-scales in a multi-estep procedure in which the transfer inter-scale function is determined by algebraic reconstruction. For comparison purposes a low pass filter is used as blurring matrix in coordination with the down-sampling scale. For example a blurring low pass filter for a down-sampling factor $q\downarrow$ is a *Butterworth* filter with cut off π/q. A high order filter is used simulating a ideal filter appropriate for the down sampling factor. In other experiment the H_r image is first blurred with a Gaussian kernel of 7×7 with standard deviation 1.6, and then down-sampled by a total scaling factor q in both horizontal and vertical directions.This blurring kernel has been used for comparison purposes. Tables 2, 3 and 4 show the enhanced result of the procedure when the downsampled factor q grow. The result of the ART convergence and gradient regularization improves the bicubic interpolation by 0.1 of SSIM and 2 dB of PSNR respectivelly. This characteristic is used as compensation of the decreasement of SSIM in dictionary SR procedures when the factor q increases. Table 5 shows that the proposed model ART-ARG improves the results of dictionary based SR methods when is used as input. Our model incorporates finally a procedures similar to the exposed in [34], the similar patches in the image are grouped, then, the values of the SR image are estimated. This procedure is applied after the multi scale scheme with ART reconstruction and the gradient management procedure ARG. The figure 6 shows visual results of the proposed algorithm, cuantitative results are in the table 5.

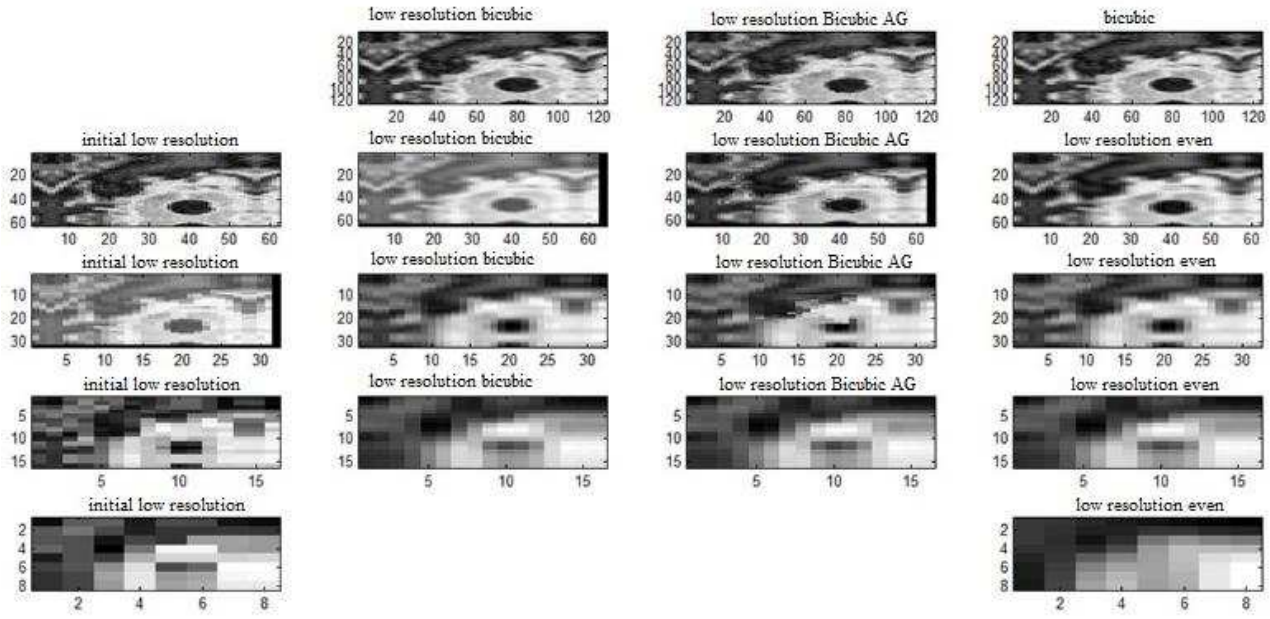

Figure 5. *The right column is the multi-scale image to determine the transfer function, in the left are the images in which the transfer function is applied*

Comparisons

When a transfer function is attained by using the ART procedure, the solution of the system is passed to the original input image and the blurring and down-sampled versions. A new image is obtained as a lineal combination of the multi-scale scheme with patches p of 2×2 pixels. Each blurred and down-sampled version of the original image is up-sampled up to the size of the input image for convenience for the solution of the linear dependence of the system. The model is determined for a number of images at different scales f_n where $f_{n=0}$ is the image of major dimension. The input image is decomposed in patches expressed in vector form, each vector has the intensity of the image in some scale. The number of dimensions of the space in which the system converge is the same as the number of scales. The solution with ART of the system with four scales of patches in the multi-scale scheme is transferred to a stair in which the input image is part of the linear system. The resulting image is restricted by gradient management ARG usig the input image in with the middle of the dimensions of the output scale.

Recently some models in [14] and [15] employ neural networks in SR for wise selection of high frequency residuals. In [14], the residuals are added to the L_r input image in order to obtain the H_r. The model in [14], as a variation of a SRResNet model, is trained with large databases of patches expanded with rotations and scale changes. In other case as [15] the residual is obtained by a discrimination between the generated H_r images and natural H_r images. Nevertheless the procedures are learning based with high dependence respect to the training database. Our proposed model learn transitions between images at different scales in the first step. The second step sharp the edges and finally the non local redundancies of the image are exploited in a procedure similar to [34]. The first and second steps in our procedure in general bring an improved start point to the search of the H_r target image. The method ART-AG-Dic in the table 5 shows results exploiting non local redundancies in a self-learning model over the ART-AG input. For comparison purposes some pictures of the BSD100 database where used. The input L_r images in the figure 7 where blurred with a 7×7 Gaussian kernel of standard deviation 1.6 and downsampled with the scale factor q=4 , the comparative results are exposed in the table 6. The tables show the gain of PSNR and SSIM of each method over the bicubic interpolation. The factors of the SSIM function are set to $K = [0.08, 0.075]$, L=255 and as *window* a gausian function of size 11×11 with standard deviation 1.5. [15].

SSIM and PSNR Comparison between ART in multiscale scheme and Bicubic using ideal and Gaussian filter $q = 4$

Image	ART-AG-Gaussian	ART-AG-Ideal	ART-AG	Bicubic-Ideal	Bicubic-gausian
MRI	0.5159/20.1542	**0.5442/20.7134**	0.5375/19.8770	0.4704/19.3473	0.4653/19.1646
Parrot	0.7532/21.9303	**0.7724/22.6622**	0.7831/23.1668	0.7268/21.6142	0.7218/21.2390
Butterfly	0.6994/18.7745	**0.7061/19.0437**	0.7168/18.5980	0.6400/17.3273	0.6468/17.2759
Bike	0.5585/19.1223	**0.5930/19.4463**	0.5726/19.1671	0.5454/18.8259	0.5193/18.4691
Flower	0.6249/21.7186	**0.6478/21.8859**	0.6407/20.7525	0.5888/20.9486	0.5706/21.2659
Hat	0.6873/21.8936	**0.6939/22.1162**	0.7024/22.6052	0.6588/21.3713	0.6651/21.4860
Leaves	0.6653/17.2703	**0.6779/16.6972**	0.7047/17.2172	0.5897/14.8963	0.6064/15.9750
Parthenon	0.6094/19.2974	**0.6199/20.0517**	0.6155/19.0261	0.5669/19.4270	0.5746/18.7921
Raccon	0.6142/23.1942	**0.6365/24.6002**	0.6110/23.3934	0.5988/23.7784	0.5811/22.3983
Plants	0.6908/23.7673	**0.7206/24.7448**	0.7248/24.3239	0.6712/23.4711	0.6583/23.0557

Note: Bold values indicate the best result

SSIM and PSNR Comparison between ART and ART-AG in multiscale scheme with Bicubic and Bicubic AG using ideal filter $q = 3$

IMAGE	Bicubic	ART-AG	ART	Bicubic-AG
MRI	0.5625/20.0699	**0.6662/21.9490**	0.5474/20.0000	0.6577/21.6009
Parrot	0.8209/23.3733	0.8163/22.1230	**0.8211/23.8170**	0.8149/22.2983
Butterfly	0.7385/19.1058	0.7286/17.4485	**0.7453/19.4559**	0.7328/17.3198
Bike	**0.6752/20.1229**	0.6640/19.5992	0.6633/19.9633	0.6650/20.0680
Flower	0.7210/21.9816	**0.7365/23.5687**	0.7082/23.0862	0.7246/23.6506
Hat	0.7354/23.2050	**0.7539/24.9170**	0.7345/23.4018	0.7509/24.2403
Leaves	0.7604/17.6857	**0.7625/18.1403**	0.7619/18.4069	0.7406/17.3743
Parthenon	0.6737/20.9178	**0.6809/21.5093**	0.6762/20.3886	0.6710/21.5197
Raccon	0.6974/24.8972	**0.6983/25.5202**	0.6912/25.2470	0.6846/24.9388
Plants	**0.7939/25.8034**	0.7933/25.2914	0.7847/25.3768	0.7926/25.2600

Note: Bold values indicate the best result

SSIM and PSNR Comparison between ART and ART-AG in multiscale scheme with Bicubic and Bicubic AG using ideal filter $q = 2$

IMAGE	ART-AG	ART	Bicubic-AG
MRI	0.6339/20.3673	0.7689/24.0406	**0.7961/24.9940**
Parrot	0.8517/22.8112	0.8925/26.6157	**0.9027/26.9642**
Butterfly	0.8010/19.1013	0.8504/22.2310	**0.8709/22.4231**
Bike	0.7366/19.9941	0.7875/21.5722	**0.8134/21.0549**
Flower	0.7842/21.9724	0.8328/24.8604	**0.8535/25.4536**
Hat	0.8007/23.7145	0.8265/26.8091	**0.8467/27.0477**
Leaves	0.7147/15.2721	0.8864/22.1044	**0.8955/20.7986**
Parthenon	0.6627/19.3558	0.7905/21.7771	**0.8022/23.6815**
Raccon	0.7812/23.2568	0.7997/27.2481	**0.8288/27.3592**
Plants	0.7538/18.6833	0.8823/28.2905	**0.9032/29.1216**

Note: Bold values indicate the best result

SSIM and PSNR Comparison between Dictionary learning methods and learning over ART-ARG $q = 4$

Image	ART-AG-Dic	NCSR [34]	ASDS-AR-NL [31]	ASDS [31]	ASDS-AR [31]
MRI	19.6817/**0.5601**	19.2359/0.5543	19.4252/0.5434	**19.8012**/0.5459	19.7430/0.5460
Parrot	**23.3360/0.8343**	23.0441/0.8309	19.4706/0.7443	19.9855/0.7498	19.8345/0.7474
Butterfly	20.0018/0.8068	**20.0826/0.8096**	17.5604/0.7186	17.0569/0.7096	16.9183/0.7100
Bike	**20.4400/0.6838**	20.2663/0.6774	20.2748/0.5929	19.4270/0.5838	19.7818/0.5876
Flower	**22.3529/0.7360**	21.6910/0.7310	22.6148/0.6369	21.7744/0.6285	22.1029/0.6296
Hat	**26.5762/0.8013**	26.2645/0.7992	24.1121/0.7473	24.9591/0.7497	24.8346/0.7484
Leaves	**20.7147/0.8242**	20.6845/0.8238	15.9664/0.6762	16.2065/0.6608	16.1773/0.6620
Parthenon	19.2777/0.6320	**19.3093/0.6331**	18.6136/0.6133	19.4370/0.6155	19.3224/0.6131
Raccon	24.0135/**0.6215**	23.3931/0.6129	**24.2312**/0.6156	24.1558/0.6134	24.1418/0.6125
Plants	22.1135/**0.7003**	22.0201/0.6977	**23.0643**/0.6975	21.8284/0.6776	22.1254/0.6810

Note: Bold values indicate the best result

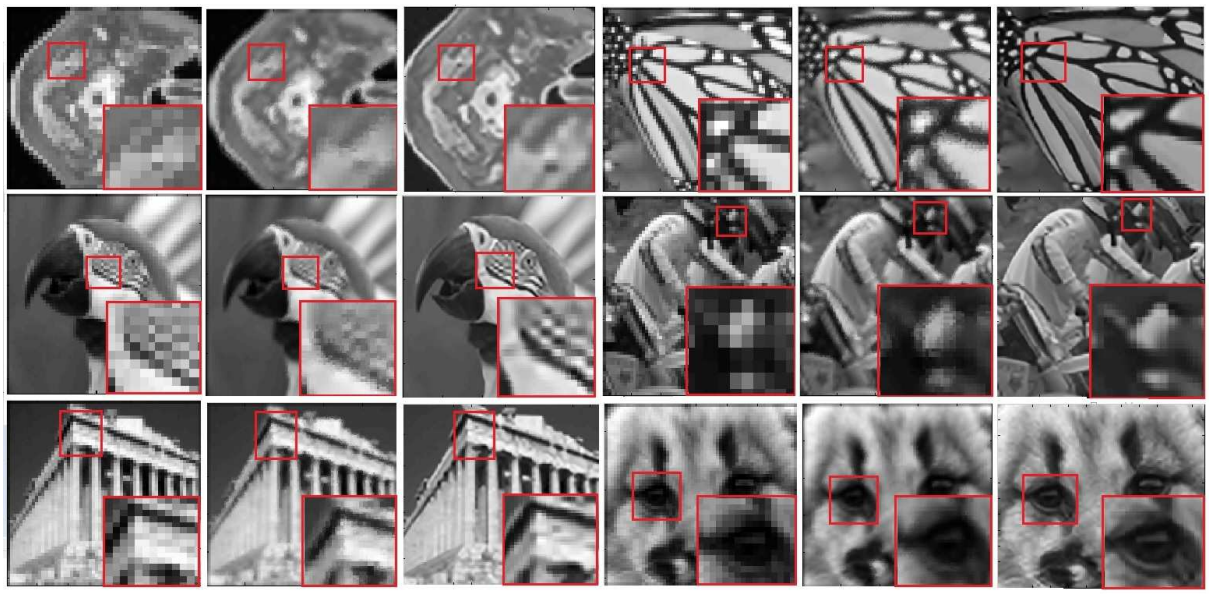

Figure 6. *In the figure the imput image, the ART-ARG and the ART-ARG-Dictionary results are showed consecutively with scale factor q=4*

Figure 7. *In the figure, left to right, the imput image, the ART-ARG and the ART-ARG-Dictionary over figures 1)idols, 42)Boys 56)Firefighter and 75)Farm of BSD100 database using factor q=4. The H_r image is first blurred with a 7×7 Gaussian kernel with standard deviation 1.6, and then down-sampled by a total scaling factor q in both horizontal and vertical directions. The PSNR/SSIM gains of our proposed method ART-AG-Dic over bicubic interpolation in each case are 1) 0.6dB/0.07 2) 1.8dB/0.06 3) -0.16dB/0.03 4) 1.5dB/0.07.*

Conclusions

In this paper, a new SR method was presented. The model ART is used to determine the transfer function between scales in a multi scale scheme of amplification. The output image of the multi-scale scheme is improved by using a new auto regularized gradient model in which a restriction of the gradient sharpness of the output image is made respect to the sharpness in a previous scale. The model shows a stability in the SSIM and PSNR ratios respect to an ideal H_r image for large sacales of amplification with $q = 4$. The method compensates and enhance the response of dictionary-based SR methods for high amplification factors. The ART model applied could be controlled by iteration in the process of the transfer function determination. The procedure is independent of external databases. The gradients auto regularization in

Gain of PSNR and SSIM over bicubic interpolation for differents methods using the database BSD100 [43] and [44] with factor $q = 4$

Method	Set 5 [43]	Set 14 [44]	BSD100
SRCNN [39]	1.64/0.04	1.19/0.03	0.74/0.035
SelfEx [40]	1.9/0.05	1.46/0.04	0.89/0.04
DRCN [41]	3.09/0.07	2.03/0.05	1.37/0.05
ESPCN [42]	2.33/0.05	1.66/0.05	1.02/0.05
SRResNet	**3.62**/0.08	**2.4**/0.069	**1.5**/0.065
SRGAN [15]	0.97/0.02	0.03/-0.008	-0.8/-0.025
ART-AG-Dic	2.01/**0.08**	1.5/**0.072**	0.6/**0.07**

Note: Bold values indicate the best result

the output image of the ART procedure makes sharpen edges.The dictionary method like [34] then carry out a best estimation of the H_r image using the ART-AG model as input and increases the SSIM and PSNR ratios over some powerful procedures reported in the state of the art. The proposed model can be useful for segmentation and 3D representation. In future work, we aim to test the proposed SR system using different transformation such as contourlets, bandelets, wavelets, dual tree and double density wavelets transform. Our system can help in the prediction of high frequency bands, also other transference configurations for multiscale amplification schemes can be investigated.

References

[1] A. Papoulis, *Systems and Transforms with Applications in Optics*, McGraw-Hill, New York, p. 105, 1966

[2] Hakran K.,et al. Curvature Interpolation Method for Image Zooming, *Image Processing. IEEE Transaction*, volume 20 (issue: 7), 2011.

[3] Liu Xianming, Zhao Debin , Xiong Ruiqin, Siwei Ma. Image Interpolation Via Regularized Local Linear Regression, *IEEE Transactions on Image Processing.*, volume 20 (issue 12), 2011.

[4] T. Lu, R. Hu, Z. Han, J. Jiang and Y. Xia, "Robust super-resolution for face images via principle component sparse representation and least squares regression," 2013 IEEE International Symposium on Circuits and Systems (ISCAS2013), Beijing, 2013, pp. 1199-1202

[5] S. Chao, X. Chun-bo and L. Shao-lei, "Improved super-resolution algorithm of single-frame image based on least square method," 2013 25th Chinese Control and Decision Conference (CCDC), Guiyang, 2013, pp. 2648-2651.

[6] W. Nam and S. H. Kong, "Least-Squares-Based Iterative Multipath Super-Resolution Technique," in IEEE Transactions on Signal Processing, vol. 61, no. 3, pp. 519-529, Feb.1, 2013

[7] X. Li and T. Q. Nguyen, Markov random ?eld model-based edgedirected image interpolation, *IEEE Trans. Image Process.*, vol. 17, no. 7, pp. 11211128, Jul. 2008.

[8] L. Zhang and X. Wu, An edge-guided image interpolation algorithm via directional ?ltering and data fusion, IEEE Trans. Image Process., vol. 15, no. 8, pp. 22262238, Aug. 2006

[9] X. Li and M. T. Orchard, New edge-directed interpolation, *IEEE Trans. Image Process.*, vol. 10, no. 10, pp. 15211527, Oct. 2001.

[10] P. Thvenaz, T. Blu, and M. Unser, Image interpolation and resampling, in *Handbook of Medical Imaging*, Processing and Analysis. Orlando, FL, USA: Academic Press, Inc., 2000, pp. 393420.

[11] H. S. Hou and H. C. Andrews, Cubic splines for image interpolation and digital ?ltering, *IEEE Trans. Acoust. Speech Signal Process.*, vol. 26, no. 6, pp. 508517, Dec. 1978.

[12] W. T. Freeman, T. R. Jones, and E. C. Pasztor, Example-based superresolution, *IEEE Comput. Graph. Appl.*, vol. 22, no. 2, pp. 5665, Mar. Apr. 2002.

[13] W. T. Freeman, E. C. Pasztor, and O. Carmichael, Learning low-level vision, *Int. J. Comput. Vision*, vol. 40, no. 1, pp. 2547, Jun. 2000.

[14] Bee Lim, Sanghyun Son, Heewon Kim, Seungjun Nah, Kyoung Mu Lee; Enhanced Deep Residual Networks for Single Image Super-Resolution, The IEEE Conference on Computer Vision and Pattern Recognition (CVPR) Workshops, 2017, pp. 136-144.

[15] Christian Ledig, et al. Photo-Realistic Single Image Super-Resolution Using a Generative Adversarial Network, The IEEE Conference on Computer Vision and Pattern Recognition (CVPR) Workshops, 2017, pp. 136-144.

[16] K. Kim and Y. Kwon, Example-based learning for singleimage SR and JPEG artifact removal, *Max Planck'Insitut fur biologische Kybernetik*, Tbingen, Germany Tech. Rep. 173, 2008.

[17] D. Glasner, S. Bagon, and M. Irani, Super-resolution from a single image, in Proc. Int. Conf. Comput. Vision, 2009, pp. 349356.

[18] J. Yang, J. Wright, Y. Ma, and T. Huang, Image super-resolution as sparse representation of raw image patches, in Proc. IEEE Conf. Comput. Vision Pattern Recognit., Jun. 2008, pp. 18.

[19] H. Chang, D.-Y. Yeung, and Y. Xiong, Super-resolution through neighbor embedding, in Proc. IEEE Conf. Comput. Vision Pattern Recognit., Jun.Jul. 2004, pp. 275282.

[20] G. Freedman and R. Fattal, Image and video upscaling from local selfexamples, ACM Trans. Graph., vol. 28, no. 3, pp. 110, 2010.

[21] M. Irani and S. Peleg., Motion analysis for image enhancement: Resolution, occlusion and transparency, *J. Visual Commun. Image Representation*, vol. 4, no. 4, pp. 324335, 1993.

[22] S. Baker and T. Kanade, Limits on super-resolution and how to break them, *IEEE Trans. Pattern Anal. Mach. Intell.*, vol. 24, no. 9, pp. 11671183, Sep. 2002.

[23] Y.-W. Tai, S. Liu, M. S. Brown, and S. Lin, Super resolution using edge prior and single image detail synthesis, in Proc. *IEEE Conf. Comput. Vision Pattern Recognit.*, Jun. 2010, pp.

24002407.
[24] R. Fattal, Image upsampling via imposed edge statistics, *ACM Trans. Graph.*, vol. 26, no. 3, pp. 95:195:8, 2007.
[25] S. Dai, M. Han, W. Xu, Y. Wu, and Y. Gong, Soft edge smoothness prior for alpha channel super resolution, in Proc. IEEE Conf. Comput. Vision Pattern Recognit., Jun. 2007, pp. 18.
[26] H. A. Aly and E. Dubois, Image up-sampling using total-variation regularization with a new observation model, *IEEE Trans. Image Process.*, vol. 14, no. 10, pp. 16471659, Oct. 2005.
[27] B. S. Morse and D. Schwartzwald, Image magni?cation using level set reconstruction, in Proc. *IEEE Conf. Comput. Vision Pattern Recognit.*, Dec. 2001, pp. 333340.
[28] J. Sun, Z. Xu, and H.-Y. Shum, Gradient pro?le prior and its applications in image super-resolution and enhancement, *IEEE Trans. Image Process.*, vol. 20, no. 6, pp. 15291542, Jun. 2011.
[29] D. Glasner, S. Bagon, and M. Irani, Super-resolution from a single image, in *Proc. IEEE Int. Conf. Comput. Vis.*, Sep./Oct. 2009, pp. 349356.
[30] A. M. Bruckstein, D. L. Donoho, and M. Elad, From sparse solutions of systems of equations to sparse modeling of signals and images, *SIAM Rev.*, vol. 51, no. 1, pp. 3481, 2009.
[31] W. Dong, L. Zhang, G. Shi, and X. Wu, Image deblurring and superresolution by adaptive sparse domain selection and adaptive regularization, *IEEE Trans. Image Process.*, vol. 20, no. 7, pp. 18381857, Jul. 2011.
[32] M. Elad and M. Aharon, "Image Denoising Via Sparse and Redundant Representations Over Learned Dictionaries," IEEE Transactions on Image Processing, Dec 2006, **15**, (12), pp. 3736 – 3745
[33] X. Zhang, M. Burger, X. Bresson, and S. Osher, "Bregmanized nonlocal regularization for deconvolution and sparse reconstruction," Soc. Ind. Appl. Math. J. Imaging Sci., 2010, **3**, (3), pp. 253 – 276,
[34] W. Dong et al, Nonlocally Centralized Sparse Representation for Image Restoration, *IEEE Trans. Image Process.*, VOL. 22, NO. 4, pp 1620-1630, April. 2013.
[35] L. Wang, S. Xiang, G. Meng, H. Wu, and C Pan, "Edge-Directed Single-Image Super-Resolution via Adaptive Gradient Magnitude Self-Interpolation," *IEEE Trans. Circ. Syst. Vid.*, vol. 23, no. 8, pp. 1289-1299, Jan. 2013.
[36] Y. Zhang et al,Image Super-Resolution Based on Structure-Modulated Sparse Representation,IEEE TRANSACTIONS ON IMAGE PROCESSING, VOL. 24, NO. 9, SEPTEMBER 2015
[37] M. C. Yang and Y. C. F. Wang, "A Self-Learning Approach to Single Image Super-Resolution," in IEEE Transactions on Multimedia, vol. 15, no. 3, pp. 498-508, April 2013
[38] Y. Sun, G. Gu, X. Sui, and Y. Liu, "Compressive Superresolution Imaging Based on Local and Nonlocal Regularizations," *IEEE Photonics J.*, vol. 8, no. 1, pp. 1-12, Jan. 2016.
[39] C. Dong, C. C. Loy, K. He, and X. Tang. Learning a deep convolutional network for image super-resolution. In European Conference on Computer Vision (ECCV), pages 184199. Springer, 2014.
[40] J. B. Huang, A. Singh, and N. Ahuja. Single image super-resolution from transformed self-exemplars. In IEEE Conference on Computer Vision and Pattern Recognition (CVPR), pages 51975206, 2015.
[41] J. Kim, J. K. Lee, and K. M. Lee. Deeply-recursive convolutional network for image super-resolution. In IEEE Conference on Computer Vision and Pattern Recognition (CVPR), 2016.
[42] W. Shi, J. Caballero, F. Huszar, J. Totz, A. P. Aitken, R. Bishop, D. Rueckert, and Z. Wang. Real-Time Single Image and Video Super-ResolutionUsinganEf?cientSub-PixelConvolutionalNeural Network. In IEEE Conference on Computer Vision and Pattern Recognition (CVPR), pages 18741883, 2016.
[43] M. Bevilacqua, A. Roumy, C. Guillemot, and M. L. Alberi-Morel. Low-complexitysingle-imagesuper-resolutionbasedonnonnegative neighbor embedding. BMVC, 2012
[44] R. Zeyde, M. Elad, and M. Protter. On single image scale-up using sparse-representations. In Curves and Surfaces, pages 711730. Springer, 2012

] Leandro Morera. Received the B.S degree in Telecomunications and M.S in Bioengineering from ISPJAE institute in Havana. He is currently pursuing the Ph.D. degree in Computer Sciences at the Center of Research and Technological Development (CENIDET). His fields of interest include pattern recognition, digital image processing, and computer vision.

Raúl Pinto Elías is an Industrial Electrical Engineer by Instituto Tecnológico de Chetumal, México (1990). He obtained the M. Sc. degree in Computer Science at the Center of Research and Technological Development (CENIDET) in 1993. He graduated as Ph.D. in Electrical Engineering from the Center for Research and Advanced Studies of the National Polytechnic Institute (CINVESTAV), México in 2000. He currently serves as a Professor at CENIDET.

Humberto de Jesús Ochoa Domínguez (M'97) received his BS degree in industrial electronics from the Technological Institute of Veracruz, México, his MSc degree in electronics from the Technological Institute of Chihuahua, Mex-

ico, and PhD degree in electrical engineering from the University of Texas at Arlington, USA. He is a full-time professor at the Universidad Autónoma de Ciudad Juárez. His current teaching and research interests include image superresolution, image and video coding, statistical shape analysis, and pattern recognition.

JOIN US AT THE NEXT EI!

IS&T International Symposium on

Electronic Imaging

SCIENCE AND TECHNOLOGY

Imaging across applications . . . Where industry and academia meet!

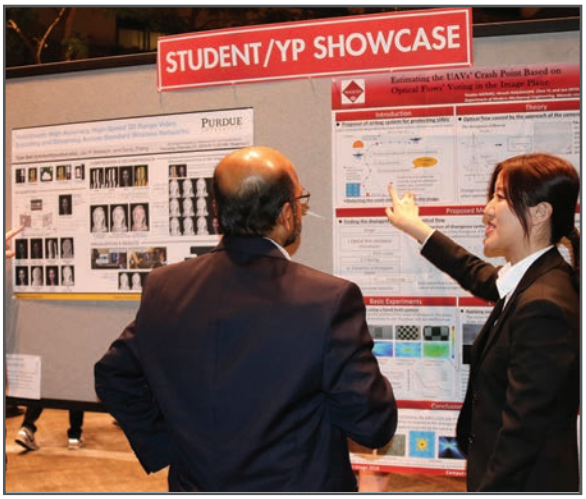

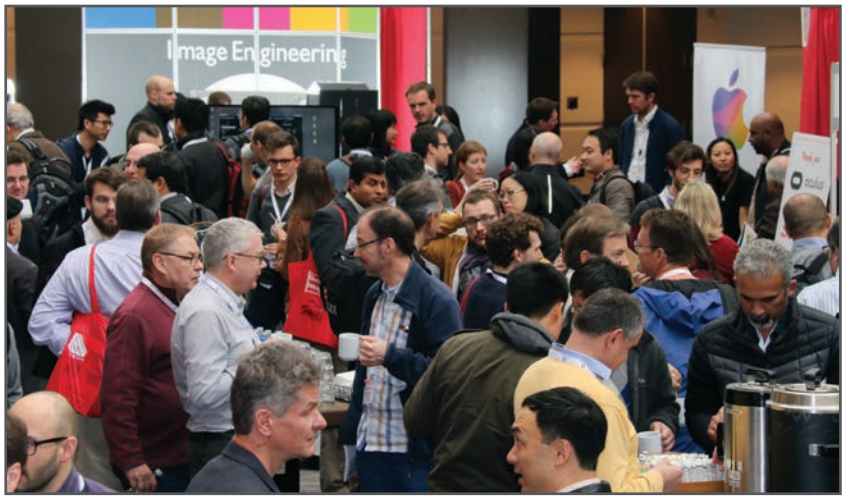

• SHORT COURSES • EXHIBITS • DEMONSTRATION SESSION • PLENARY TALKS •
• INTERACTIVE PAPER SESSION • SPECIAL EVENTS • TECHNICAL SESSIONS •

www.electronicimaging.org

IS&T
imaging.org